

The EVP method revisited

Sylvain Bouillon^a, Gurvan Madec^{b,c}, Thierry Fichefet^a, Vincent Legat^{a,d}

^a*Georges Lemaître Centre for Earth and Climate Research, Earth and Life Institute, Université catholique de Louvain, Louvain-la-Neuve, Belgium*

^b*Laboratoire d'Océanographie et du Climat: Expérimentation et Approches Numériques (LOCEAN), Paris, FRANCE*

^c*National Oceanography Centre, Southampton (NOCS), United Kingdom*

^d*Institute of Mechanics, Materials and Civil Engineering, Université catholique de Louvain, Louvain-la-Neuve, Belgium*

Abstract

The Elastic-Viscous-Plastic method (EVP) is revisited as a non-linear solver dedicated to the Viscous-Plastic dynamics model (VP). A clear distinction appears between the physical parameters of the model and the numerical parameters. Two numerical parameters control the stability and the convergence rate of the solver. A third parameter gives the termination criterion either in terms of the residual of the is theoretically analysed and demonstrated in a real case simulation.

The stability and the convergence analysis Impacts of numerical parameters on the convergence, the stability and the simulated deformation field are investigated.

Key words: viscous-plastic rheology, elastic-viscous-plastic, sea ice, C-grid, NEMO

Email addresses: sylvain.bouillon@uclouvain.be (Sylvain Bouillon)

Preprint submitted to Ocean Modelling

1. Introduction

Most sea ice models use some variant of the viscous-plastic (VP) rheology (Hibler, 1979) and give realistic drift pattern. Simulations at high resolution does not performed very well in reproducing the deformation field especially at small spatial and temporal scales (Kwok et al. (2008) and Girard et al. (2009)).

It raises questions about the principal assumptions on which plastic models have been build (Coon et al., 2007) and it generates a regain of interest to build up a new framework for sea ice dynamics as in Girard et al. (2011), Hibler and Schulson (2000), Wilchinsky and Feltham (2004) and Schreyer et al. (2006). Some authors still claim that with a high enough resolution and a correct solving method, the VP rheology is able to simulate high deformation bands similar to what is observed in reality (Wang and Wang (2009) and Maslowski and Lipscomb (2003)).

Several methods are used to solve the non-linear VP rheology. One of the most famous method is the elastic-viscous-plastic (EVP) method that is thoroughly documented in Hunke (2001); Hunke and Dukowicz (1997, 2002), and Hunke and Lipscomb (2008). Other numerical methods have been developed as in Lemieux et al. (2012) and Zhang and Rothrock (2000). Several methods have been proposed to solve the VP rheology. Hibler (1979) proposed an implicit treatment of the momentum equation with viscosities computed from velocities of the last time step but it suffers very slow convergence towards the ellipse. Sub-iterations or smaller time step have been used to the detriment of the computational cost and without a fast enough convergence rate as shown by Lemieux and Tremblay (2009). Another approach is to iteratively solve the non-linear set of equations by the Newton method as in Lemieux et al. (2012). But the most popular method is the EVP method proposed by Hunke and Dukowicz (1997) where an additional elastic term is added to the constitutive law (3) to allow an explicit solving of the momentum equation while keeping a stable scheme. All those methods are based on sub-iterations performed within each global time step. The number of sub-iterations may be fixed or automatically adapted to reach a certain degree of convergence either in terms of stresses or ice velocities.

We work in the framework of the NEMO sea ice-ocean model (?) which is discretised on a C-grid. will modified the discretisation of the EVP method implemented by Bouillon et al. (2009b) in the LIM2 version of the sea ice model (see Madec et al. (1998) and Fichefet and Maqueda (1997) for the

other aspects of the LIM2 model).

The VP rheology has the property to dissipate energy. The spatial discretisation is build to preserve that property. VP equations are solved by a modified EVP method that ensures a good solution even.

2. The Viscous-Plastic Model and its dissipative property

The VP rheology and the continuous sea ice dynamics are coupled by a constitutive equation defining the internal stress tensor $\boldsymbol{\sigma}$ as a function of the derivatives of the ice velocity and the 2D momentum equation equation:

$$\begin{aligned} 0 &= \boldsymbol{\sigma} - \mathbf{g}(\mathbf{u}) \\ m \partial_t \mathbf{u} &= \nabla \cdot \boldsymbol{\sigma} + \mathbf{f}(\mathbf{u}) \end{aligned} \quad (1)$$

where m is the combine mass of snow and ice per unit area and \mathbf{u} the horizontal ice velocity.

The momentum equation is obtained by integrating the 3D momentum equation through the thickness of the snow and ice in the vertical direction. The momentum advection is being ignored in (1) and all the terms that do not depends on the internal stress are grouped in $\mathbf{f}(\mathbf{u})$ by

$$\mathbf{f}(\mathbf{u}) = a(\boldsymbol{\tau}_a + \boldsymbol{\tau}_w) - m f \mathbf{k} \times \mathbf{u} - m g \nabla \phi_o. \quad (2)$$

The wind stress $\boldsymbol{\tau}_a$ and the ocean stress $\boldsymbol{\tau}_w$ are multiplied by the ice concentration a (Connolley et al., 2004). $\boldsymbol{\tau}_a$ is an external forcing and $\boldsymbol{\tau}_w$ is given by a quadratic expression $c_D \rho_o |\mathbf{u}_o - \mathbf{u}|^{s-1} (\mathbf{v}_o - \mathbf{v})$. The other two terms are stresses due to Coriolis effects and due to the sea surface slope.

The constitutive law proposed by Hibler (1979) relates the internal ice stress σ_{ij} and the rates of strain $\epsilon_{ij} = \frac{1}{2}(\frac{\partial u_i}{\partial x_j} + \frac{\partial u_j}{\partial x_i})$ by

$$\begin{aligned} \sigma_1 &= P \frac{(D_D - \Delta)}{(\Delta + \Delta_{min})} \\ \sigma_2 &= \frac{P}{e^2} \frac{D_T}{(\Delta + \Delta_{min})} \\ \sigma_{12} &= \frac{P}{2e^2} \frac{D_S}{(\Delta + \Delta_{min})} \\ \Delta &= \sqrt{D_D^2 + \frac{1}{e^2} (D_T^2 + D_S^2)} \end{aligned} \quad (3)$$

where

$$\begin{aligned}
\sigma_1 &= \sigma_{11} + \sigma_{22} \\
\sigma_2 &= \sigma_{11} - \sigma_{22} \\
D_D &= \epsilon_{11} + \epsilon_{22} \\
D_T &= \epsilon_{11} - \epsilon_{22} \\
D_S &= 2\epsilon_{12}
\end{aligned} \tag{4}$$

and Δ_{min} is the parameter determining the transition from viscous to plastic deformation.

In the pure plastic case when $\Delta \gg \Delta_{min}$, equation 3 corresponds to an elliptical yield curve in the stress state space. The compressive stress σ_1 and the shearing stress $\sigma_s = (\sigma_2^2 + 4\sigma_{12}^2)^{0.5}$ are related through the quadratic expression $(\sigma_1 + P)^2 + e^2\sigma_s^2 = P^2 \frac{D_D^2}{\Delta^2} + e^2 \frac{P^2}{e^2} \frac{D_T^2 + D_S^2}{\Delta^2} = P^2$. The length of the major axis corresponds to the maximum compressive stress $2P$. e is the ratio between the major axis and the minor axis. The ellipse is not centred on the origin but translated into the $\sigma_1 \leq 0$ part of the stress space. The ice pack is assumed having no resistance to pure divergence but resist compression and shearing motion in the other cases.

The response of the ice is plastic. It does not depend on the magnitude of the deformation rate but only on the direction of the strain rate vector defined by the shear strain rate $\sqrt{D_T^2 + D_S^2}$ and divergence strain rate D_D . Each possible stress state on the ellipse corresponds to a certain direction of the strain rate vector. This constitutive law respects the normal flow rule because the strain rate vector will always be normal to the yield curve in principal stresses and strain rates plane. P is measure of ice strength that depends on thickness and compactness by $P = P^* a h e^{c^*(1-a)}$, where P^* and c^* are empirical constants and h is the mean ice thickness (in our case $P^* = 10^4 Nm^{-2}$ and $c^* = 20$). Other constitutive laws with a different yield curve or another flow rule may be used but this combination of the ellipse yield curve and the normal flow rule is very popular and will be used in this paper.

One of the main characteristics of the VP rheology is the dissipation of energy. We will develop that property from the continuous equations and it will help in defining a correct spatial discretisation for the VP equations in the following.

Table 1: Symbols used in the text

Symbol	Definition	Units
P	ice pressure (strength)	N m^{-1}
M	mass of snow and ice per unit area	Kg m^{-2}
h	mean ice thickness	m
a	ice concentration	-
Δ	measure of the deformation rate	s^{-1}
D	rate of internal work	N m s^{-1}
D_D	Divergence	s^{-1}
D_S	shearing strain rate	s^{-1}
D_T	tension strain rate	s^{-1}
$\mathbf{F} = (F_u, F_v)$	stress divergence	N m^2
ϵ_{ij}	component of the strain rate tensor	s^{-1}
σ_{ij}	component of the stress tensor	N m^2
$\mathbf{U} = (u, v)$	ice velocity	m s^{-1}

$$\begin{aligned}
D &= -\frac{1}{2} \iint_S (D_D \sigma_1 + D_T \sigma_2 + 2D_S \sigma_{12}) dS \\
&= -\iint_S \frac{P}{2\Delta} \left(D_D (D_D - \Delta) + \frac{1}{e^2} (D_T^2 + D_S^2) \right) dS \\
&= -\iint_S \frac{P}{2\Delta} \Delta (\Delta - D_D) dS \\
&= -\iint_S \frac{P}{2} (\Delta - D_D) dS
\end{aligned} \tag{5}$$

As Δ is obviously larger or equal to D_D and $P \geq 0$, D is always negative or zero. Therefore, the work of internal ice force over the ice pack is to dissipate energy. This dissipation of energy is a fundamental property of the VP rheology. It is important to preserve this property in the discretisation such that the discrete system dissipates energy in the same manner as the continuous system (Hunke and Dukowicz, 2002).

3. Discretisation and the EVP method

The spatial discretisation is the same as presented in Bouillon et al. (2009a). It is based on the C-grid arrangement of variables with cells centred on scalar points (t -points) and velocity points (u - and v -points) defined in the centre of each face of the cells. σ_1 and σ_2 are defined on t points as well as D_D and D_T . σ_{12} and D_S are defined on the corner of the cells (f -points). This arrangement minimizes the need of averaging operator for the evaluation of the different derivatives by the finite difference method. Only two variables have to be interpolated. D_S is needed on (t -points) to compute Δ and Δ on (f -points) to compute σ_{12} . The average operators have to be of that form: $\ll D_S^2 \gg_t$ and $\ll \frac{1}{\Delta} \gg_f$ to satisfy the property of energy dissipation (??)(see annex). Any linear combination of Δ on f -point and any linear combination of D_S on t -points will fail in satisfying the dissipation of kinetic energy constraint. Those operators are the only differences with the spatial discretisation presented in Bouillon et al. (2009a).

3.1. The temporal discretisation

To illustrate the temporal discretisation the following simplified one-dimensional version of the VP equation will be used:

$$\begin{aligned} 0 &= \frac{P}{2\Delta} \partial_x u - \sigma \\ M \partial_t u &= \partial_x \sigma + f \\ \Delta &= |\partial_x u| \end{aligned} \tag{6}$$

The simplest discretisation is an explicit scheme to advance in time from time step n to time step $n + 1$ using:

$$M \frac{u_{n+1} - u_n}{\Delta t} = \partial_x \frac{P}{2\Delta_n} \partial_x u_n + f \tag{7}$$

The stability criterion scales quadratically with Δx as

$$\Delta t \leq \frac{M\Delta}{P} \Delta x^2 \tag{8}$$

Because the deformation rate Δ can be as small as $10^{-9} s^{-1}$. In that case and with a spatial resolution $\Delta x = 50km$, $P = 20000N/m$ and $M \sim 1000kg m^{-2}$,

the order of magnitude of the required time step would be 10 s. To enhance larger time step, implicit scheme are preferred.

VP equations are non-linear. Newton's method has been recently used (Lemieux et al., 2010) but in most sea ice models the solving of those non linear equation is based on outer loop iterations (Zhang and Hibler, 1997). Within each outer loop iteration ($s + 1$) a linearised version of the equation is solved. In our simple case, Δ would be computed with velocity from the previous outer loop iteration (s).

$$M \frac{u_{n+1}^{m+1} - u_n}{\Delta t} = \partial_x \frac{P}{2\Delta_{n+1}^m} \partial_x u_{n+1}^{m+1} + f \quad (9)$$

. The main drawback of this method is the slow convergence towards the solution. Even with 40 outer loop the velocity field can have significant error as shown by Lemieux and Tremblay (2009). Within each outer loop a solver is called to solve the linear system of equation (GRES, LSOR, ...).

The EVP method developed by Hunke (2001) and the modified EVP approach (Lemieux et al., 2012) can be interpreted as a a fixed iteration point iteration method. This approach aims at finding u_{n+1} and σ_{n+1} that satisfy the VP implicit equations rewritten as

$$\begin{aligned} \mathbf{G}(\mathbf{u}, \sigma) &= \mathbf{g}(\mathbf{u}_{n+1}) - \sigma_{n+1} = 0 \\ \mathbf{F}(\mathbf{u}, \sigma) &= \nabla \cdot \sigma_{n+1} + \hat{\mathbf{f}}(\mathbf{u}_{n+1}) = 0 \end{aligned} \quad (10)$$

where $\hat{\mathbf{f}}(u) = \hat{\mathbf{f}}(u) - M\partial_t \mathbf{u}$.

A each iteration an approximate solutions \mathbf{u}^{m+1} and σ^{m+1} is generated from the \mathbf{u}^m and σ^m . The objective is to converge to the solution of (10) by successively executed those operations:

$$\sigma^{m+1} = \sigma^m - \frac{\mathbf{G}(\mathbf{u}^m), \sigma^m}{G'} \frac{1}{\alpha} \mathbf{u}^{m+1} = \mathbf{u}^m - \frac{\mathbf{F}(\mathbf{u}^m), \sigma^{m+1}}{F'} \frac{1}{\beta} \quad (11)$$

where α and β are two adimensional parameters and G' and F' are approximate derivatives of each equation with respect to the respective variable.

$$\begin{aligned} G' &= -1 \\ F' &= -\frac{M}{\Delta t} \end{aligned} \quad (12)$$

Name	T [s]	Δt [s]	Δt_e [s]	α	β
Hunke (b)	1296	3600	30	43.2	120
Hunke (a)	1296	3600	3	432	1200
Lemieux	432	1200	30	14.4	40
Lemieux	432	1200	10	4.8	120

Table 2: Values of the numerical parameters for each experiment. Exp1 uses the standard values.

This method looks like the Newton’s method but in a much simpler form. G' and F' are a very crude approximation of the Jacobian and each variables are decoupled. No solver are needed as each variables are decoupled.

The algorithm presented here is exactly equivalent to the generalized EVP method if

$$\alpha = \frac{T}{\Delta t_e} \tag{13}$$

$$\beta = \frac{\beta* \Delta t}{M \Delta t_e}$$

where T is the elastic time parameter, $\beta*$ is the extra inertial tuning parameter, Δt_e is the sub iteration time step and Δt is the global time step. It also corresponds to the standard EVP method if $\beta* = M$ and if the number of iteration is fixed at $n_{evp} = \frac{\Delta t}{\Delta t_e}$. In that case β corresponds to n_{evp} .

α and β control the speed of convergence to the solution while their product controls the stability of the method. Those two parameters are very useful to compare EVP simulations made in different configurations. For example the test-case of Hunke (2001) with $\Delta t_e = 3$ s and with the ratio $\frac{\alpha}{\beta}$

In Hunke test case the ratio $\frac{\alpha}{\beta}$ is the same (0.36) in both experiments but the product is much smaller in the experiment (b). The oscillation in the divergence field is better explained by a lack of stability than by a problem of convergence. In Lemieux et al. (2012) the product is the same and the better convergence is observed with the smaller value for α .

The termination criterion can be a maximum number of iteration or depends on a measure of the residual in function of $\mathbf{G}(\mathbf{u}^m, \sigma^m)$ and $\mathbf{F}(\mathbf{u}^m, \sigma^m)$. In our experiments the error is either defined as the maximum velocity update between two iterations $max(\|u^{m+1} - u^m\|, \|v^{m+1} - v^m\|)$ over all the domain, either as the norm of the difference in velocity with an approximate

solution obtained with a much larger number of iteration. We also evaluate the error by the distance of the stress state with regard to the yield curve and by the difference in the shear and the divergence rate field with a solution obtained with more iterations. In our case the termination criterion is fixed by a maximum number of iterations.

The method is consistent meaning that if $(\mathbf{u}^m), \sigma^m$ is solution of (10) $(\mathbf{u}^{m+1}), \sigma^{m+1}$ given by (11) is equal to $(\mathbf{u}^m), \sigma^m$.

To analyse the convergence it is convenient to interpret the solving process as the evolution of the approximate solution in function of a dimensionless variable s . (11) corresponds to an explicit discretization of a partial differential set of equations. One iteration corresponds to one step Δs with $\Delta s = 1$.

In the one dimensional case the iterative process corresponds to

$$\begin{aligned}\alpha \partial_s \sigma &= \frac{P}{2\Delta} \partial_x u - \sigma \\ \beta \partial_s u &= \left(\partial_x \sigma + \hat{f} \right) \frac{\Delta t}{M} \\ \Delta &= |\partial_x u|\end{aligned}\tag{14}$$

Combining both equations leads to a wave equation

$$\partial_s^2 u = \frac{\gamma}{\alpha\beta} \partial_x^2 u - \frac{1}{\alpha} \partial_s u\tag{15}$$

where $\gamma = \frac{P}{2\Delta} \frac{\Delta t}{M}$. Δ is considered constant and non homogeneous terms have been dropped. From this equation two adimensional numbers are defined:

$$\begin{aligned}S_e &= \sqrt{\frac{\alpha\beta}{\gamma}} \Delta x \\ S_v &= \frac{\beta}{\gamma} \Delta x^2\end{aligned}\tag{16}$$

. S_e is the spring, it drives the approximation towards the solution. S_v is the dashpot, it limits the update of the approximation. S_e could also be interpreted as an elastic pseudo time scale and S_v as a viscous pseudo time scale. It explains the name of the EVP method and the confusion with the VP model. The ratio $\xi = \frac{S_e}{S_v} = \sqrt{\frac{\alpha\gamma}{\beta\Delta x^2}}$ determines the damping. Oscillations occur during the approach of the solution only if $\xi > 1$.

Following Hunke (2001) the approximate solution evolves as $e^{i(kx-\omega s)}$ where $i = \sqrt{-1}$, k is the wave number ($k \leq \frac{1}{\Delta x^2}$) and ω the damping rate which is a complex number obtained by the dispersion relation:

$$\omega^2 + \frac{1}{\alpha}i\omega - \frac{\gamma k^2}{\alpha\beta} = 0 \quad (17)$$

. The damping is controlled by the imaginary part of w that is given by

$$w = \frac{1}{2\alpha} \left(-i - \sqrt{\frac{\xi - 1}{\alpha}} \right) \quad (18)$$

. If $\xi > 1$ the convergence rate is controlled by $\frac{1}{2\alpha}$ and oscillations preclude local convergence. If $\xi < 1$, the convergence rate given by $\frac{1}{2\alpha} \left(1 + \sqrt{\frac{1-\xi}{\alpha}} \right)$ is higher and local convergence is allowed.

Following the analysis made by Hunke (2001), the stability criterion is $2S_e > \Delta s$ where $\Delta s = 1$.

In cases where internal stress vanishes, under divergence or in region with lower concentration, the problem reduces to

$$\beta \partial_s u_{n+1} = -c u_{n+1} + d \quad (19)$$

where d regroups all the terms independent of u_{n+1} and c is a linearisation of the implicit term given by $c = 1 + \rho_0 c_D |u - u_o| \frac{\Delta t}{M}$ where ρ_0 the water mass density, c_D is the water drag coefficient and u_o is the oceanic surface velocity. The solution is approach as $e^{-\frac{c}{\beta}s}$. In the worst case $c = 1$ and the convergence is controlled by $\frac{1}{\beta}$.

To summarize: α and β are two adimensional parameters controlling the stability and the convergence of the method. Both are ≥ 1 .

In high internal stress areas the convergence is faster with low α . The product of α and β controls the stability by the criterion $S_e > \frac{1}{2}$. The local convergence is controlled by their ratio and is allowed if $\xi < 1$. The residual approximately decreases as $e^{-\frac{m}{2\alpha}}$ in both cases.

In low internal stress areas the convergence is faster with low β . The method is always stable and locally convergent The residual decreases as $e^{-\frac{m}{\beta}}$ where m is the number of performed iterations.

The first part of the exponential decay of the residual observed in Lemieux (ok) is a bit faster than $e^{-\frac{s}{\beta}}$ but it is even slower after 1500 iterations.

Name	α	β	S_e	S_v	ξ
Hunke (ko)	43.2	120	0.02	$0.06 \cdot 10^{-4}$	2600
Hunke (ok)	432	1200	0.16	$0.62 \cdot 10^{-4}$	2600
Lemieux (ko)	14.4	40	0.08	$4.8 \cdot 10^{-4}$	170
Lemieux (ok)	4.8	120	0.08	$15 \cdot 10^{-4}$	57

Table 3: Values of the numerical parameters for each experiment. Exp1 uses the standard values.

Name	P^*	Δt	Δ_{min}	γ
Hunke	27500	3600	10^{-11}	$4950 \cdot 10^{12}$
Lemieux	27500	1200	$2 \cdot 10^{-9}$	$8.25 \cdot 10^{12}$

Table 4: Values of the numerical parameters for each experiment. Exp1 uses the standard values.

The stability will be endanger with the smallest value of Δ which is defined by Δ_{min} . In both paper this lowest value is observed during the simulation and could then be used to verified the stability criterion and the damping criterion. concentration equal or near to 1, $P = P * h e^{-c(1-a)}$, $M \simeq \rho_i h$, $\gamma = \frac{P * \Delta t}{2 \Delta_{min} \rho_i}$

At the first iteration ($m = 1$) an initial guess have to be defined. We take zero for σ_1 , σ_2 and σ_{12} and the ice velocity at the previous time step \mathbf{u}_n . It avoids the propagation of a ill resolved stress state from one time step to another. Other initial guess as the free drift velocity for \mathbf{u} or a smooth version of the previous velocity could be used to limit the propagation of undamped oscillations.

To summarize: EVP is a non-linear solver developed for solving equations (10) obtained from the implicit time discretisation of the VP model. Convergence rate and stability of this simple fixed point iteration method are controlled by two numerical parameters. With the stability criterion and the damping ratio, they entirely defined the behaviour of the solver and offer a simple way to compare different implementations of the EVP method in

different configurations. The parallelisation is trivial but the convergence is not very high and underdamped solution could generate great problems when coupling with the ice thickness redistribution.

In previous implementations of the EVP method, numerical and physical term were mixed up. The numerical terms were interpreted as an artificial inertial mass and artificial elastic term generating some confusion between the numerical method and the physical model. The number of iteration n_{evp} was a constant and Δs had to be equal to $\frac{\Delta t}{n_{evp}}$. The generalized EVP method suppresses the need of a fixed number of iterations by separating the solving of the physical inertial term to the update of the velocity between to sub-iterations.

The stress update terms also differ a little in comparison with standard EVP. For σ_1 , $\alpha = \frac{2T}{\Delta t_e}$ with T the elastic time parameter and Δt_e the pseudo time step defined in previous studies. For σ_1 and σ_{12} , it would be $\alpha = \frac{1}{e^2} \frac{2T}{\Delta t_e}$ to really corresponds to the standard EVP method. Keeping the same α for the three equation has a surprisingly good impact on the convergence as it will be showed in the next section.

The whole algorithm is described hereafter to give all details.

Within the iterative process, variables indexed with m are updated while variables indexed with n are referred to the global time step and stay constant.

At each solver iteration, the internal stress tensor on the C-grid is updated first by

$$\begin{aligned}\alpha(\sigma_1^{m+1} - \sigma_1^m) &= P \frac{(D_D^m - \Delta^m)}{\Delta^m} - \sigma_1^m \\ \alpha(\sigma_2^{m+1} - \sigma_2^m) &= \frac{P D_T^m}{e^2 \Delta^m} - \sigma_2^m \\ \alpha(\sigma_{12}^{m+1} - \sigma_{12}^m) &= \frac{P D_S^m}{2e^2 \Delta^m} - \sigma_{12}^m\end{aligned}\tag{20}$$

The internal force vector is then computed by

$$\mathbf{F}^{m+1} = (F_u^{m+1}, F_v^{m+1}) = \nabla \cdot \sigma^{m+1}\tag{21}$$

The update of u and v is decoupled. On odd iterations, (22) is solved first with v^* being an interpolation of v^m on u-point et u^* equal to u^{m+1} , then (23) is solved with $v^* = v^{m+1}$ et u^* is u^{m+1} interpolated on v-point.

The inverse order is applied for even iterations.

$$\beta(u^{m+1} - u^m) = (F_u^{m+1} - \frac{M}{\Delta t}(u^{m+1} - u_n) + A(\tau_{\mathbf{a}u} + c_D \rho_o |\mathbf{u}_o - (u^*, v^*)|(u_o - u^{m+1})) + M f v^*) \frac{\Delta}{M} \quad (22)$$

and

$$\beta(v^{m+1} - v^m) = \left(F_v^{m+1} - \frac{M}{\Delta t}(v^{m+1} - v_n) + A_v \{ \tau_{\mathbf{a}u} + c_D \rho_o |\mathbf{u}_o - (u^*, v^*)|(v_o - v^{m+1}) \} - M f u^* \right) \frac{\Delta}{M} \quad (23)$$

c_D is the water drag coefficient, ρ_o the water mass density and $\mathbf{u}_o = (u_o, v_o)$ the horizontal sea surface velocity.

4. Analysis

The computational time to solve sea ice dynamics a strict convergence is almost never reached for sea ice dynamics in climate model and both numerical parameters and physical parameters may have an impact on the simulated fields.

The two numerical parameters α and β and the number of iterations m . The other constraints are the convergence of the stress state, the convergence in term of velocity and the stability criterion.

In this section we study the impact of α and β different aspects of the simulated deformation field.

persistence of spurious deformation in near rigid regions as in the Canadian Arctic Archipelago that is caused by a lack of convergence in stresses and/or a problem of stability.

All the results presented in this section are produced with an ice-only version of NEMO (standalone version of the LIM2 model). Sea surface temperature and salinity come from a temporal interpolation of the Levitus98 monthly mean climatology. The ocean is at rest with no elevation. The ocean drag is defined by a quadratic formulation with a drag coefficient $C_d = 5 \cdot 10^{-3}$ and no turning angle. The wind is interpolated from the 6 hourly DFS4.1 10m wind speed. Surface boundary conditions (wind stress and other fluxes) are computed with the CORE bulk formulae developed by Large and Yeager (2004). The time step is equal to 4 hours ($\Delta t = 14400s$) and all simulations start the first of January 1991. The domain is restricted to 25°North and initial conditions are very simple, no ice wherever the sea surface temperature

Name	α	β	S_e	S_v	ξ
Exp1	49	122	0.19	$7.6 \cdot 10^{-4}$	250
Exp2	20	300	0.19	$19 \cdot 10^{-4}$	100
Exp3	63	947	0.61	$59 \cdot 10^{-4}$	100
Exp4	20	3000	0.61	$190 \cdot 10^{-4}$	33

Table 5: Values of the numerical parameters for each experiment. Exp1 uses the standard values.

is 2 degrees above the freezing point of sea water, 3 *m* of ice and 50 *cm* of snow elsewhere. The initial concentration of the ice pack is equal to 1. The ORCA05 tripolar grid has a resolution (Δx) of about 15 km in the Canadian Arctic Archipelago and around 25 km in the Central Arctic. Advection and thermodynamics LIM2 modules are activated.

We only show results for the first time step but our analysis stay valid for longer simulations. The variables of interest are the divergence and the shearing rates, as well as the stress state. We also look at the evolution of the velocity update between to successive iterations of the method, $\max(|u^s - u^{s-1}|, |v^s - v^{s-1}|)$. All simulations perform a fixed number of iterations $m_{max} = 300$.

The first simulation uses similar parameters as the standard case presented in Hunke (2001).

In our case, Δ is evaluated a posteriori from the solution. The minimum value simulated in a cell that is not on the coast or at the ice edge is around $2 \cdot 10^{-9} s^{-1}$. It is a better estimation than Δ_{min} which is in our case equal to $10^{-20} s^{-1}$. $\gamma = \frac{P*\Delta t}{2\Delta\rho_i} = 36 \cdot 10^{12}$.

Another annoying feature is the alignment of high deformation bands with the grid. It suggests that the appearance of those linear bands is more a numerical artefact than a real ability to simulate observed linear kinematic features as announced in Wang and Wang (2009) and in Maslowski and Lipscomb (2003).

The second part of the analysis concerns the sensitivity to the value of T , β and Δt_e . A smaller T improves the convergence to VP by damping out the elastic waves more rapidly. However it endangers the stability of the solution if the value of Δt_e and/or the value of β are not adapted. Stability and damping problems are the two causes of the spurious deformation in the CAA.

Name	n_{evp}	T	β	Δt_e
Exp1	300	$0.4 \Delta t$	m	$\sqrt{6} \Delta t / n_{evp}$
Exp2	300	$0.4 \Delta t / 6$	m	$\Delta t / n_{evp}$
Exp3	300	$0.4 \Delta t / 6$	m	$\frac{1}{\sqrt{10}} \Delta t / n_{evp}$
Exp4	300	$0.4 \Delta t / 6$	$10 m$	$\Delta t / n_{evp}$

Table 6: Values of the numerical parameters for each experiment. Exp1 uses the standard values.

Four experiments performed with different set of parameters are presented. All experiments were conducted with the two corrections described here above.

Exp1 use the standard parameters already presented here above (see Table 4). For Exp2, T has been divided by 6 and Δt_e by $\sqrt{6}$ to reduce residual elastic waves while keeping the same stability condition. The solution will remain stable if $\Delta > 2 \cdot 10^{-8} s^{-1}$. In Exp3, we decrease the elastic time step Δt_e to improve the stability condition. Exp3 will be stable when $\Delta > 2 \cdot 10^{-9} s^{-1}$ but it will slow down the convergence towards the ellipse because the number of sub-iterations is not large enough. In the last experiment Exp4, we increase β to improve stability (ok when $\Delta > 2 \cdot 10^{-9} s^{-1}$) while keeping the same Δt_e as in Exp2 to do not alter the convergence towards the ellipse.

To analyse the impact of those different sets of parameters, we look at the divergence rate within the CAA, at the stress state after the first global time step and at the evolution of the velocity update between successive sub-iterations. In Figure ??, the four experiments are presented from the left to the right. For Exp1, the first on the left, the stress state has not converged to the ellipse and there is remaining spurious deformation in the CAA. If we look at the evolution of the maximum velocity update (red line in Figure ??) we see oscillations that indicate stability issues.

Exp2 has a better convergence towards the ellipse thanks to a smaller value of T but suffers the same oscillating issue (blue line in Figure ??) and spurious divergence rate in the CAA. It indicates that the stability is not strong enough.

The smaller value of Δt_e in Exp3 solves the stability problem (red dashed line in Figure ??). However the convergence to the ellipse is too slow and elastic waves stay active in the CAA even if spurious deformations are reduced.

Exp4 has an optimal set of parameters. It eliminates spurious deformation in the CAA while ensuring the convergence towards the ellipse and avoiding stability issues. This is due to the small enough value of T combined with a stronger stability condition thanks to the extra-inertial term related to β . However, by slowing down the convergence in term of velocity, it acts as an additional inertial term that remains active even after 300 sub-iterations.

While being relatively limited, this analysis gives new insights in understanding how EVP method works to solve the VP rheology. First of all, we have shown how small changes in the temporal and spatial discretisation could dramatically change the appearance of linear deformation bands. Those changes should be implemented in other sea-ice models to look at their impacts in other configurations. The smoothed definition of viscosities could be tested with all the different methods (EVP, VP implicit, ...) while the new temporal scheme could only improve sea ice models based on EVP.

It indicates a more rapid convergence in the shear stress direction than in the compressive stress direction. This is due to the different treatment of the stress temporal derivatives in (20) where $\sigma_{2,t}$ and $\sigma_{12,t}$ are divided by e^2 while $\sigma_{1,t}$ is not. We propose a new evolution equation for stresses where all the stress temporal derivatives are treated in the same way:

$$\begin{aligned}
\frac{T}{\Delta t_e}(\sigma_1^s - \sigma_1^{s-1}) + \frac{1}{2}\sigma_1^{s-1} &= \zeta^{s-1} (D_D^{s-1} - \Delta^{s-1}) \\
\frac{T}{\Delta t_e}(\sigma_2^s - \sigma_2^{s-1}) + \frac{1}{2}\sigma_2^{s-1} &= \eta^{s-1} D_T^{s-1} \\
\frac{T}{\Delta t_e}(\sigma_{12}^s - \sigma_{12}^{s-1}) + \frac{1}{2}\sigma_{12}^{s-1} &= \frac{\eta^{s-1}}{2} D_S^{s-1}
\end{aligned} \tag{24}$$

The effect of this change should not have an impact on the solution if it is completely converged. It should only change the speed of convergence. However, with this first set of parameters, the solution does not completely converged to the right ellipse and we can see the effect of the new equation (24) on the evolution of the stress state. Contrary to the standard equation (20), the stress state has now the right aspect ratio throughout all the iterative process as shown in the bottom of Figure ??, meaning that the convergence rate is the same in both principal stress directions.

That little change in the iterative process produces the same filtering effect as the new definition of viscosities Δ_{smt} . The linear deformation bands completely disappear while the general pattern remains the same. On the

contrary to the change of Δ , the deformation field is not smoother except near the suppressed high deformation bands. The divergence and the shear rate in Figure ?? have been obtained with the same parameters as the standard run. The only change is new temporal stress evolution equation (24). In the CAA, the deformation field is still spurious.

The fact that a small change completely inhibit the production of high deformation bands let to numerical problems than to a real ability to reproduce the reality.

We observed the same effect for all the tested set of parameters. The filtering of high deformation bands remain similar even with better converged solutions.

The first part of the analysis gives clues to correctly choose the parameters related to the iterative solving process of the EVP method. The optimal time step eliminates spurious deformation in the CAA while giving a good convergence towards the ellipse. The stress state will converge faster and the oscillations will be more damped but the error in the approximate velocity is large. Larger β should then be limited in high internal stress areas.

5. Conclusions

In this paper we address two problems observed in high resolution simulations of the sea ice dynamics. Those two problems are clearly identified in the upper left panel of Figure ?. The first one is the high deformation bands aligned with the grid and the second one is the remaining spurious deformation in the CAA. We have shown how numerical problems could cause the appearance of those so-called "Linear Kinematics Features" aligned with the grid and how those features magically disappear with small changes in the numerics. The high deformation bands can be completely filtered out either by changing the definition of the viscosities or by changing the stress update equation to ensure the same convergence rate in the shear and the compressive stress direction as shown in the upper right panel of Figure ? where both corrections have been applied together. Both modifications conserve the energy dissipation property of the discrete equations and do not really modify the deformation field elsewhere. To mitigate the spurious deformation in near rigid ice regions, we had to tackle both the stability problem and the damping of the artificial elastic term. Thanks to new diagnostics, we found an optimal set of parameters for our configuration that severely reduced the remaining spurious deformation in the CAA (see the lower left

panel of Figure ??). Combining the corrections of the temporal and the spatial discretisation with the optimal set of parameters led to a much more stable sea ice dynamics.

Those changes will have a great impact on simulated sea ice. Especially for multi-categories sea ice models that are very sensitive to the deformation field when playing at high resolution (Lipscomb et al., 2007). It also give new insight in how the EVP method works and how it should be used. Implications of those changes on a larger timescale within a coupled sea ice-ocean model will be investigated and if they are validated in various configurations, those changes will be integrated in the standard version of LIM2 and LMIM3.

Acknowledgements. To be added : IsENES european project which support this ice work in Paris.

6. Appendix

Our main objective here is to derive a consistent discretisation of the internal ice force, *i.e.* that satisfies the property of dissipation of energy :

$$D = \int (u F_u + v F_v) dS + \text{boundary terms} \leq 0 \quad (25)$$

Introducing the discrete expression of the internal forces,

$$\begin{aligned} D &= \int_S (F_u u + F_v v) ds \\ &\equiv \sum_{i,j} \{F_u u e_{1u} e_{2u}\} + \sum_{i,j} \{F_v v e_{1v} e_{2v}\} \\ &\equiv \frac{1}{2} \sum_{i,j} \left\{ \delta_{i+1/2} [\sigma_1] + \frac{1}{e_{2u}^2} \delta_{i+1/2} [e_{2t}^2 \sigma_2] + \frac{2}{e_{1u} e_{2u}} \delta_j [e_{1f}^2 \sigma_{12}] \right\} u e_{2u} \\ &\quad + \frac{1}{2} \sum_{i,j} \left\{ \delta_{j+1/2} [\sigma_1] + \frac{1}{e_{1v}^2} \delta_{j+1/2} [e_{1t}^2 \sigma_2] + \frac{2}{e_{1u} e_{2u}} \delta_i [e_{2f}^2 \sigma_{12}] \right\} v e_{1v} \end{aligned} \quad (26)$$

Integrating D by parts,

$$\begin{aligned} D &= -\frac{1}{2} \sum_{i,j} \left\{ \delta_i [u e_{2u}] \sigma_1 + \delta_i \left[\frac{u}{e_{2u}} \right] e_{2t}^2 \sigma_2 + 2 \delta_{j+1/2} \left[\frac{u}{e_{1u}} \right] e_{1f}^2 \sigma_{12} \right\} \\ &\quad - \frac{1}{2} \sum_{i,j} \left\{ \delta_j [v e_{2v}] \sigma_1 + \delta_j \left[\frac{v}{e_{1v}} \right] e_{1t}^2 \sigma_2 + 2 \delta_{i+1/2} \left[\frac{v}{e_{2v}} \right] e_{2f}^2 \sigma_{12} \right\} \end{aligned} \quad (27)$$

introducing the discrete formulation for D_D , D_T and D_S ,

$$D = -\frac{1}{2} \sum_{i,j} \{D_D \sigma_1 + D_T \sigma_2\} e_{1t} e_{2t} - \sum_{i,j} \{D_S \sigma_{12}\} e_{1f} e_{2f} \quad (28)$$

and the following discrete formulation for σ_1 , σ_2 and σ_{12} :

$$\begin{aligned} \sigma_1 &= 2\zeta (D_D - \Delta) \\ \sigma_2 &= 2\eta D_T \\ \sigma_{12} &= \mathcal{M}(\eta) D_S \end{aligned} \quad (29)$$

where $\mathcal{M}(\cdot)$ is an operator that provide the value of t -point defined variable on a f -point. The adjoint of \mathcal{M} , \mathcal{M}^* , providing the inverse operation. D becomes

$$\begin{aligned} D &= - \sum_{i,j} \zeta \left\{ D_D (D_D - \Delta) + \frac{1}{e^2} D_T^2 \right\} e_{1t} e_{2t} - \sum_{i,j} \{ \mathcal{M}(\eta) D_S^2 \} e_{1f} e_{2f} \\ &= - \sum_{i,j} \zeta \left\{ D_D^2 + \frac{1}{e^2} \left(D_T^2 + \frac{1}{e_{1t} e_{2t}} \mathcal{M}^*(D_S^2 e_{1f} e_{2f}) - D_D \Delta \right) \right\} e_{1t} e_{2t} \end{aligned} \quad (30)$$

Defining the discretisation of Δ at t -point as

$$\Delta = \sqrt{D_D^2 + \frac{1}{e^2} \left(D_T^2 + \frac{1}{e_{1t} e_{2t}} \mathcal{M}^*(D_S^2 e_{1f} e_{2f}) \right)} \quad (31)$$

D become

$$D = - \sum_{i,j} \zeta \Delta \{ \Delta - D_D \} e_{1t} e_{2t} \leq 0 \quad (32)$$

where the inequality results from the fact that Δ is obviously larger or equal to D_D while the other terms are positive by nature.

Defining $\mathcal{M}(\cdot) = \overline{\overline{\cdot}}^{i+1/2, j+1/2}$ which is an auto-adjoint operator leads to

$$\Delta = \sqrt{D_D^2 + \frac{1}{e^2} \left(D_T^2 + (D_S^2)_f \right)} \quad (33)$$

and to interpolate $D_S^2 (P/(2\Delta))$ on t - (f -) points, as follows :

$$\begin{aligned} \mathcal{M}^*(D_S) &= \frac{1}{e_{1t} e_{2t}} \overline{\overline{D_S^2 e_{1f} e_{2f}}}^{i,j} \\ \mathcal{M}(\zeta) &= \overline{\overline{\zeta}}^{i+1/2, j+1/2} \end{aligned} \quad (34)$$

Note that another as simple solution is possible. Defining \mathcal{M} as $e_{1f} e_{2f} \mathcal{M}(\cdot) = \overline{\overline{\cdot}}^{i+1/2, j+1/2}_{e_{1t} e_{2t}}$

$$\begin{aligned} \mathcal{M}^*(D_S) &= \overline{\overline{D_S^2}}^{i,j} \\ \mathcal{M}(\eta) &= \frac{1}{e_{1f} e_{2f}} \overline{\overline{\eta}}^{i+1/2, j+1/2}_{e_{1t} e_{2t}} \end{aligned} \quad (35)$$

Note that any linear combination of Δ to compute η on f -point and/or of D_S on t -points will fail in satisfying the dissipation of kinetic energy constraint.

In the above calculation, all boundary terms than appears in the integration by part (equivalently in the application of the adjoint of discret operator) are zero.

References

- Bouillon, S., Maqueda, M. A. M., Legat, V., Fichefet, T., 2009a. An elastic-viscous-plastic sea ice mode formulated on Arakawa B and C grids. *Ocean Modelling* 27, 174–184.
- Bouillon, S., Maqueda, M. A. M., Legat, V., Fichefet, T., 2009b. An elastic-viscous-plastic sea ice model formulated on arakawa b and c grids. *Ocean Modelling* 27 (3-4), 174–184.
- Connolley, W. M., Gregory, J. M., Hunke, E., McLaren, A. J., 2004. On the consistent scaling of terms in the sea-ice dynamics equation. *J. Phys. Oceanogr.* 34, 1776–1780.
- Coon, M., Kwok, R., Levy, G., Pruis, M., Schreyer, H., Sulsky, D., 2007. Arctic ice dynamics joint experiment (aidjex) assumptions revisited and found inadequate. *Journal of Geophysical Research* 112, C11S90.
- Fichefet, T., Maqueda, M., 1997. Sensitivity of a global sea ice model to the treatment of ice thermodynamics and dynamics. *Journal of Geophysical Research* 102 (C6), 12609–12.
- Girard, L., Bouillon, S., Weiss, J., Amitrano, D., Fichefet, T., Legat, V., 2011. A new modeling framework for sea-ice mechanics based on elasto-brittle rheology. *Annals of Glaciology* 52 (57), 123–132.
- Girard, L., Weiss, J., Molines, J., Barnier, B., Bouillon, S., et al., 2009. Evaluation of high-resolution sea ice models on the basis of statistical and scaling properties of arctic sea ice drift and deformation. *Journal of Geophysical Research* 114 (C8).
- Hibler, W., 1979. A dynamic thermodynamic sea ice model. *Journal of Physical Oceanography* 9, 815–846.
- Hibler, W., Schulson, E., 2000. On modelling the anisotropic failure and flow of flawed sea ice. *Journal of Geophysical Research* 105, 17105–17120.
- Hunke, E., 2001. Viscous-plastic sea ice dynamics with the evp model: Linearization issues. *J. Comput .Phys.* 170, 18–38.
- Hunke, E., Dukowicz, J., 1997. An elastic-viscous-plastic model for sea ice dynamics. *J. Phys. Oceanogr.* 27, 1849–1867.

- Hunke, E. C., Dukowicz, J. K., 2002. The elastic-viscous-plastic sea ice dynamics model in general orthogonal curvilinear coordinates on a sphere – incorporation of metric terms. *Mon. Wea. Rev.*, 1848–1865.
- Hunke, E. C., Lipscomb, W. H., 2008. Cice: the los alamos sea ice model documentation and software user’s manual. Tech. rep., T-3 Fluid Dynamics Group, Los Alamos National Laboratory, Los Alamos NM 87545.
- Kwok, R., Hunke, E., Maslowski, W., Menemenlis, D., Zhang, J., 2008. Variability of sea ice simulations assessed with rgps kinematics. *J. Geophys. Res* 113, C11012.
- Large, W., Yeager, S., 2004. Diurnal to decadal global forcing for ocean and sea-ice models: The data sets and flux climatologies. ncar tech. Note TN-460+ STR.
- Lemieux, J., Knoll, D., Tremblay, B., Holland, D., Losch, M., 2012. A comparison of the jacobian-free newton-krylov method and the evp model for solving the sea ice momentum equation with a viscous-plastic formulation: A serial algorithm study. *Journal of Computational Physics*.
- Lemieux, J., Tremblay, B., 2009. Numerical convergence of viscous-plastic sea ice models. *J. Geophys. Res* 114, C05009.
- Lemieux, J.-F., Tremblay, B., Sedlacek, J., Tupper, P., Thomas, S., D., H., Auclair, J.-P., 2010. Improving the numerical convergence of viscous-plastic sea ice models with the jacobian-free newton-krylov method. *J. Comp. Phys.* 229, 2840–2852.
- Lipscomb, W., Hunke, E., Maslowski, W., Jakacki, J., 2007. Ridging, strength, and stability in high-resolution sea ice models. *J. Geophys. Res* 112, C03S91.
- Madec, G., Delecluse, P., Imbard, M., Lévy, C., 1998. Opa 8.1 ocean general circulation model reference manual.
- Maslowski, W., Lipscomb, W., 2003. High resolution simulations of arctic sea ice, 1979–1993. *Polar Research* 22 (1), 67–74.
- Schreyer, H. L., Sulsky, D. L., Munday, L. B., Coon, M. D., Kwok, R., 2006. Elastic-decohesive constitutive model for sea ice. *Journal of Geophysical Research* 111, C11S26.

- Wang, K., Wang, C., 2009. Modeling linear kinematic features in pack ice. *Journal of Geophysical Research* 114 (C12), C12011.
- Wilchinsky, A. V., Feltham, D. L., 2004. A continuum anisotropic model of sea-ice dynamics. *Royal Society* 460, 2105–2140.
- Zhang, J., Hibler, W. D., 1997. On an efficient numerical method for modelling sea ice dynamics. *Journal of Geophysical Research* 102, 8691–8702.
- Zhang, J., Rothrock, D., 2000. Modeling arctic sea ice with an efficient plastic solution. *Journal of geophysical research* 105 (C2), 3325–3338.

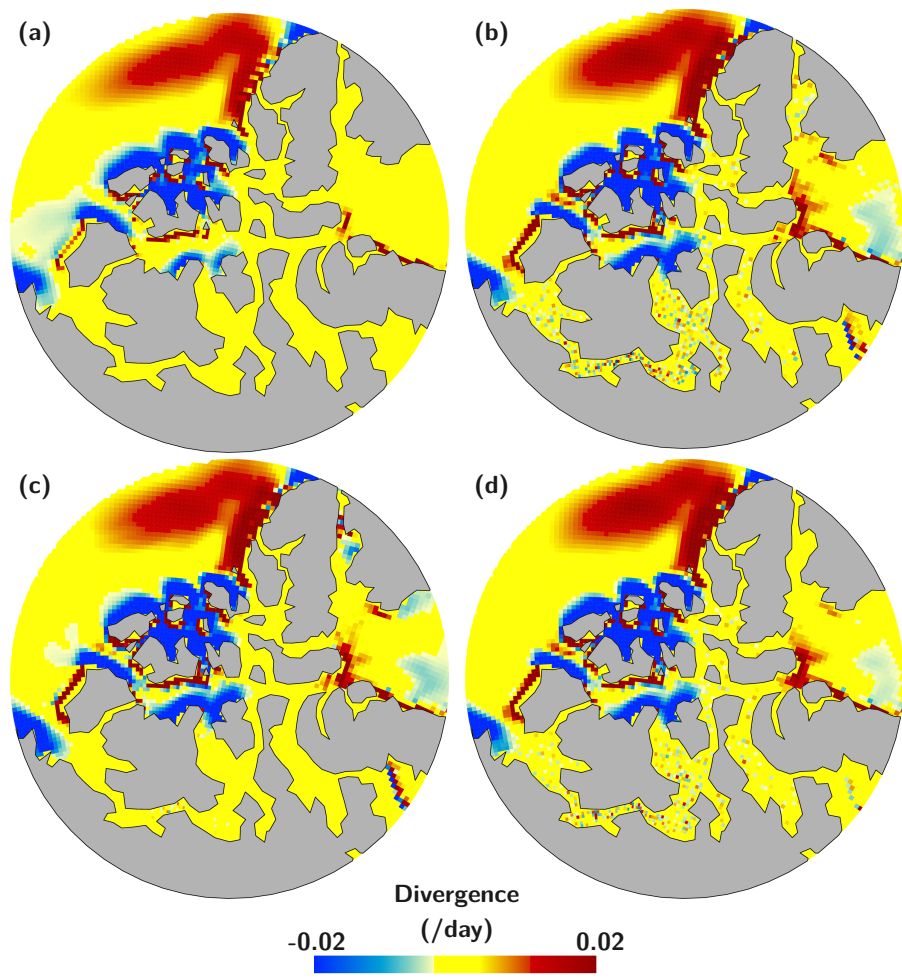


Figure 1: Divergence rate [day^{-1}] within the Canadian Arctic Archipelago after the first time step for ...

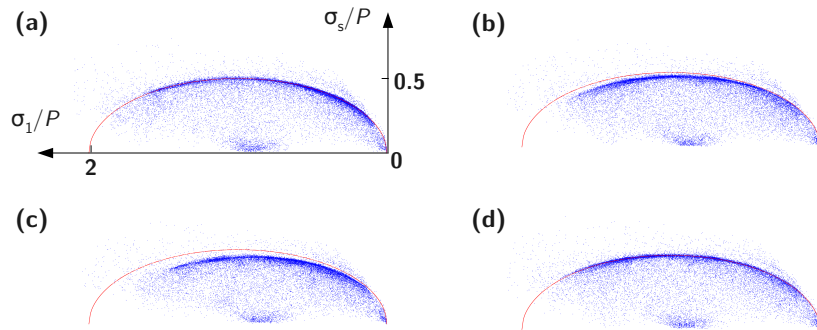


Figure 2: Normalized stress state after the first time step

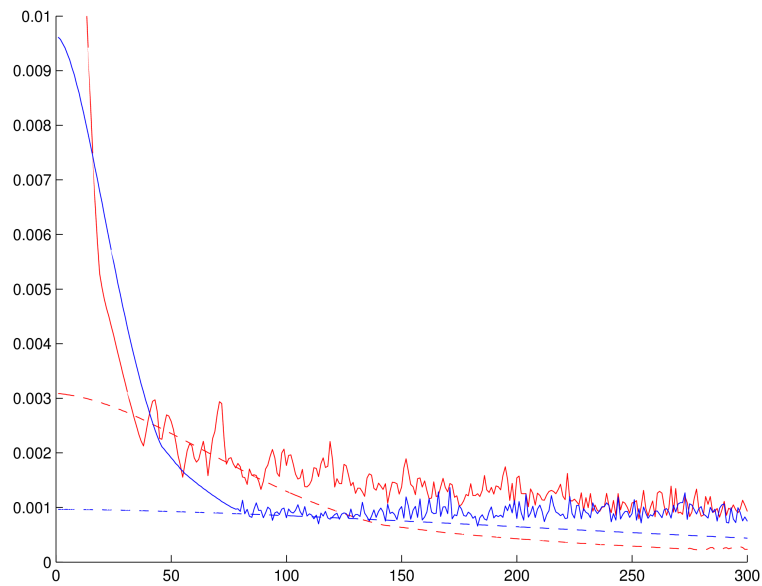


Figure 3: Evolution of the maximum difference $[m/s]$ in velocity between two iterations during the first time step. The first experience is in red, the second in blue, the third in dashed red and the last on in dashed blue.

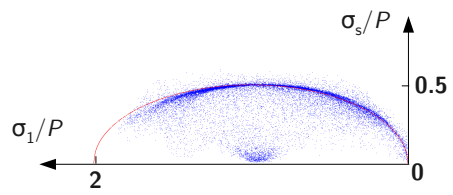


Figure 4: Normalized stress state after the first time step with β divided by e^2 for σ_2 and σ_{12} as in the standard EVP method.

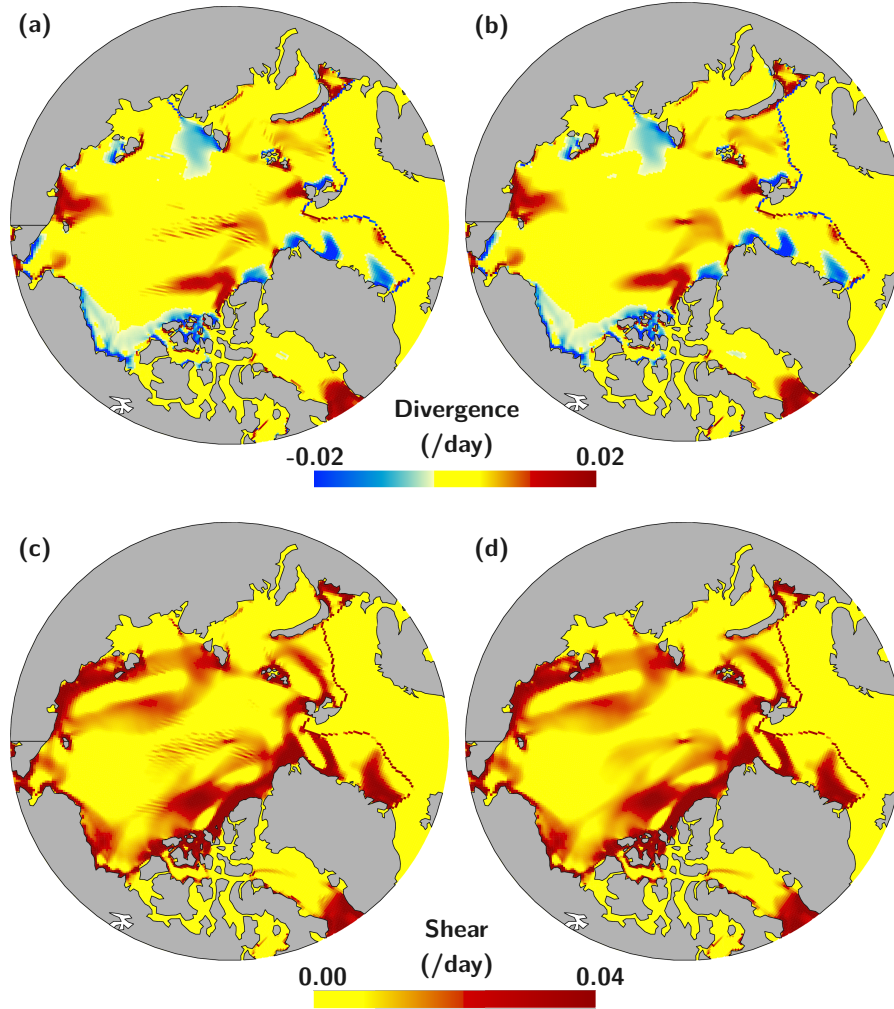


Figure 5: Figure ??: Divergence rate [day^{-1}] (top) and shear rate [day^{-1}] (bottom) after the first time step with the standard parameter $\beta = m$, $T = 0.4 \Delta t$ and $\Delta t_e = \frac{\sqrt{6}}{300} \Delta t$ with the modified (24).

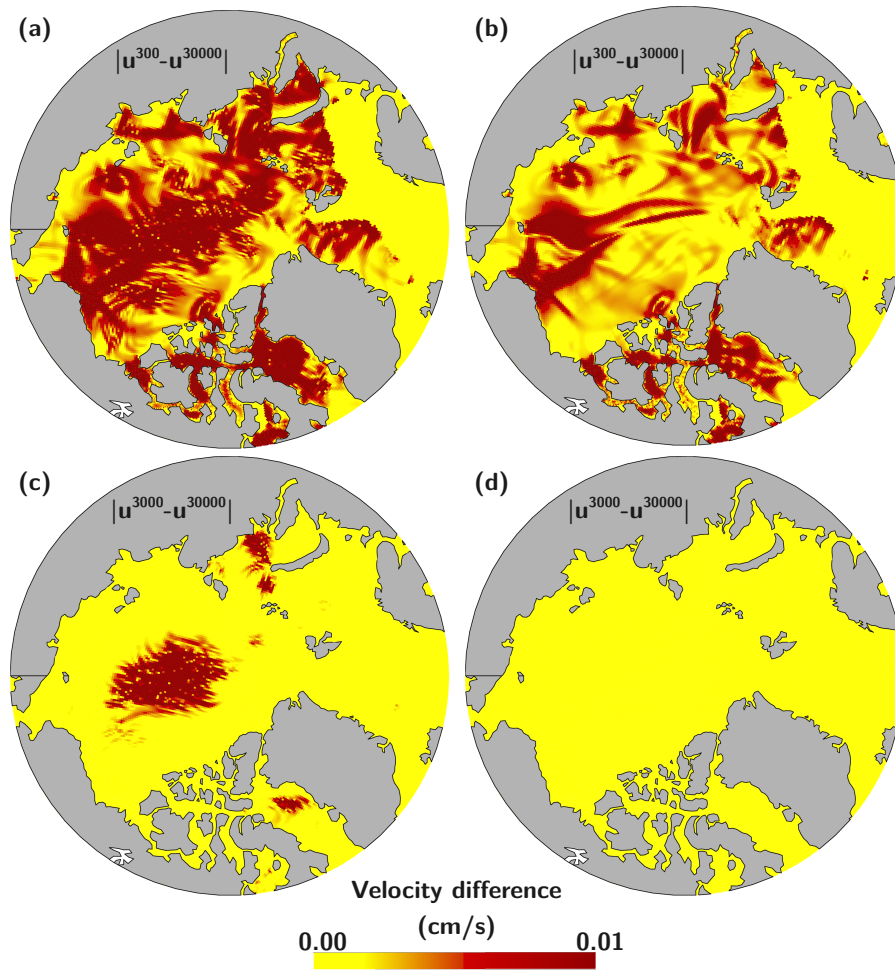


Figure 6: